arXiv:1702.06302v1 [cond-mat.str-el] 21 Feb 2017

Giant magnetoelectric effect in pure manganite-manganite heterostructures

Sanjukta Paul[1], Ravindra Pankaj[1], Sudhakar Yarlagadda[1], Pinaki Majumdar[2], and Peter B. Littlewood[3,4]
[1] *CMP Div., Saha Institute of Nuclear Physics, HBNI, Kolkata, India*
[2] *Harish-Chandra Research Institute, HBNI, Allahabad, India*
[3] *Argonne National Laboratory, Argonne IL 60439 and*
[4] *University of Chicago,James Franck Institute, Chicago IL 60637*

(Dated: February 22, 2017)

Obtaining strong magnetoelectric couplings in bulk materials and heterostructures is an ongoing challenge. We demonstrate that manganite heterostructures of the form (Insulator)/$(LaMnO_3)_n$/$(CaMnO_3)_n$/(Insulator) show strong multiferroicity in magnetic manganites where ferroelectric polarization is realized by charges leaking from $LaMnO_3$ to $CaMnO_3$ due to repulsion. Here, an effective nearest-neighbor electron-electron (electron-hole) repulsion (attraction) is generated by cooperative electron-phonon interaction. Double exchange, when a particle virtually hops to its unoccupied neighboring site and back, produces magnetic polarons that polarize antiferromagnetic regions. Thus a striking giant magnetoelectric effect ensues when an external electrical field enhances the electron leakage across the interface.

PACS numbers: 75.85.+t, 71.38.-k, 71.45.Lr, 71.38.Ht, 75.47.Lx, 75.10.-b

I. INTRODUCTION

Complex oxides such as manganites display a rich interplay of various orbital, charge, and spin orders when rare-earth dopants are added to the parent oxide. While significant progress has been made in characterizing the bulk doped materials, the heterostructures produced from two parent oxides is an area of active research[1,2]. In these heterostructures, the accompanying quantum confinement, anisotropy, heterogeneity, and the enhanced gradients (in magnetic moments, electric potential, orbital polarization, etc.) across the interface result in novel phenomena that have no counter part in the bulk samples[3]. In fact, the challenge is to technologically exploit this new physics and develop new useful devices that can meet future demands such as miniaturization, dissipationless operation/manipulation (such as read/write capability), energy storage, etc[4–10].

There has been a revival in multiferroic research partly due to improved technology, discovery of new compounds (such as $YMnO_3$, $TbMn_2O_5$), need for devices with strong magnetoelectric effect, etc[11]. Majority of the multiferroics studied are bulk materials where it is not yet clear why the magnetic and electric polarizations coexist poorly[12]. With the advent of improved molecular-beam-epitaxy technology one can now grow oxide heterostructures with atomic-layer precision and explore the possibility of strong multiferroic phenomena as well as large interplay between ferroelectricity and magnetic polarization. Coupling between the charge and spin degrees of freedom is fascinating both from a fundamental viewpoint as well as from an applied perspective. Instead of employing currents and magnetic fields, controlling and manipulating magnetism with electric fields holds a lot of promise as the electric fields are easier to use in smaller dimensions and can potentially lower energy consumption in systems. There are numerous mechanisms for magnetoelectric effect; reviews for these can be found in Refs. 13–17. At the interface of a magnetic oxide and a ferroelectric/dielectric oxide, magnetoelectric effect of electronic origin has been predicted by some researchers. Upon application of an external electric field, not only the magnitude of moments can be changed[18,19], but in some cases the very nature of magnetic ordering can be changed[20].

Among various efforts pertaining to oxide heterostructures, there is considerable interest, both experimentally[21–28] as well as theoretically[29–34], in understanding novel aspects of conductivity, magnetism, and orbital order in pure manganite-manganite $TMnO_3/DMnO_3$ heterostructures where T refers to trivalent rare earth elements La, Pr, Nd, etc. and D refers to divalent alkaline elements Sr, Ca, etc. At low temperatures, the bulk $TMnO_3$ is an insulating A-type antiferromagnet (A-AFM); on the other hand, the bulk $DMnO_3$ is an insulating G-type antiferromgnet (G-AFM). Furthermore, the doped alloy $T_{1-x}D_xMnO_3$ is an antiferromagnet for $x > 0.5$; whereas for $x < 0.5$, it is a ferromagnetic insulator (FMI) at smaller values of x (i.e., $0.1 \lesssim x \lesssim 0.2$)[35–37] and is a ferromagnetic metal at higher dopings in $La_{1-x}Sr_xMnO_3$, $La_{1-x}Ca_xMnO_3$, $Pr_{1-x}Sr_xMnO_3$, and $Nd_{1-x}Sr_xMnO_3$. For representative studies of doped manganite-manganite heterostructures, the reader is referred to Ref. 38.

In spite of considerable efforts towards control of magnetization through electric fields in multiferroic bulk materials and heterostructures, obtaining strong magnetoelectric couplings continues to be a challenge. Here, in this paper, we predict a novel giant magnetoelectric effect, not at the interface, but away from it, in a pure manganite-manganite heterostructure (see Fig. 1). Our objective is to present a plausible multiferroic phenomenon in manganite heterostructures and point out the associated unnoticed striking magnetoelectric effect. Cooperative electron-phonon interaction is shown to be key to understanding both multiferroicity and magne-

toelectric effect in our oxide heterostructure. Here, we exploit the fact that manganites have various competing phases that are close in energy and that by using an external perturbation (such as an electric or a magnetic field) the system can be induced to alter its phase. We show that there is a charge redistribution (with a net electric dipole moment perpendicular to the interface) and a concomitant ferromagnetism due to the optimization produced by the following two competing effects: (i) energy cost to produce holes on the $LaMnO_3$ (LMO) side and excess electrons on the $CaMnO_3$ (CMO) side; and (ii) energy gain due to electron-hole attraction (or electron-electron repulsion) on nearest-neighbor Mn sites induced by electron-phonon interaction. The charge polarization is akin to that of a pn-junction in semiconductors although the governing equations are different. The key results of our analysis are as follows: (i) the interface charge density at the LMO-CMO interface is 0.5 electrons/site. The LMO-CMO interface is ferromagnetic and persists to be ferromagnetic for another layer adjacent to the interface on the LMO side; (ii) minority carriers leak across the interface of the heterostructure and produce ferromagnetic domains due to the ferromagnetic coupling (generated by electron-phonon interaction and double-exchange) between an electron-hole pair on adjacent sites; and (iii) since ferroelectricity and ferromagnetism have a common origin [i.e., minority carriers or holes (electrons) on LMO (CMO) side], there is a striking interplay between these two polarizations; consequently, when an external electric field is applied to increase minority carriers, a giant magnetoelectric effect results.

The rest of the paper is organized as follows. In Sec. II we introduce our phenomenological Hamiltonian (based on cooperative electron-phonon-interaction physics) using which we deduce the charge distribution in the continuum approximation. We also provide a simple analytic treatment for the magnetic profile and demonstrate a giant magnetoelectric effect in a few-layered heterostructure. Next, in Sec. III, we adopt a more detailed numerical approach and introduce a Hamiltonian that includes additional kinetic terms, work functions, and discrete lattice effects. Here, magnetoelectric effect is studied in symmetric lattices (involving equal number of LMO and CMO layers) as well as in asymmetric lattices using Monte Carlo simulations. We close in Sec. IV with our concluding observations.

II. ANALYTIC TREATMENT

We will begin our treatment of the pure manganite-manganite heterostructure by considering a simple analytic picture in this section. In the next section, we will take recourse to a more detailed numerical approach.

A. Polaronic Hamiltonian

In our (Insulator)/$(LaMnO_3)_n$/$(CaMnO_3)_n$/(Insulator) heterostructure depicted in Fig. 1, due to charge leaking across the LMO-CMO interface, we expect different states of the phase diagram of $La_{1-x}Ca_xMnO_3$ (LCMO) at different cross-sections perpendicular to the growth direction. Since far from the LMO-CMO interface the material properties must be similar to those in the bulk, we expect the $x = 0$ phase at the Insulator-LMO interface and the $x = 1$ phase at the other end involving CMO-Insulator interface. Considering majority of the LCMO phase diagram (including the end regions near $x = 0$ and $x = 1$) is taken up by insulating phases, since band width is significantly diminished at strong electron-phonon coupling, and because the heterostructures are quasi two-dimensional (2D), we expect that there is no effective transport in the direction normal to the oxide-oxide interface (i.e., the z-direction). Then, for analyzing the charge distribution normal to the interface, the starting polaronic Hamiltonian is assumed to comprise of localized electrons and have the following phenomenological form:

$$H_{\rm pol} \sim -\sum_{j,\delta}\left[\gamma^1_{\rm ep} g^2\omega_0 + \frac{\gamma^2_{\rm ep} t^2_{j,j+\delta}}{g^2\omega_0}\right] n_j(1-n_{j+\delta}), \quad (1)$$

where the first coefficient $\gamma^1_{\rm ep} g^2\omega_0$ is due to electron-phonon interaction and represents nearest-neighbor electron-electron repulsion brought about by incompatible distortions of nearest-neighbor oxygen cages surrounding occupied Mn ions. The pre-factor $\gamma^1_{\rm ep}$ can depend on the phase – for instance, in the regime of C-type antiferromagnet (C-AFM) in LCMO, $\gamma^1_{\rm ep}$ is expected to be large because occupancy of neighboring d_{z^2} orbitals is inhibited in the z-direction; while in the regime of A-AFM (corresponding to undoped $LaMnO_3$), $\gamma^1_{\rm ep}$ is expected to be weaker because of compatible Jahn-Teller distortions on neighboring sites. Here, we will assume for simplicity that $\gamma^1_{\rm ep}$ is concentration independent and that $0.1 \le \gamma^1_{\rm ep} \le 1$. Next, the coefficient $\gamma^2_{\rm ep} t^2/(g^2\omega_0)$ results from processes involving hopping to nearest-neighbor and back and is present even when we consider the simpler Holstein model[39] or the Hubbard-Holstein model[40]. The pre-factor $\gamma^2_{\rm ep}$ varies between 1/2 (for non-cooperative electron-phonon interaction) and 1/4 (since for cooperative breathing mode in one-dimensional chains $\gamma^2_{\rm ep} = 1/3$, which should be more than in C-chains)[41]. Now, even within the two-band picture of manganites in Ref. 42, the electrons in the localized polaronic band contribute the term $t^2/g^2\omega_0$; the broad band (due to undistorted states that are orthogonal to the polaronic states) is an upper band whose band width is reduced due to the 2D nature of the system and does not overlap with the polaronic band to produce conduction even at carrier concentrations corresponding to $0.2 \lesssim x \lesssim 0.5$. Furthermore, although n_j is the total number in both the orbitals at site j, it can only take a maximum value of 1 due

to strong on-site electron-electron repulsion and strong Hund's coupling. Next, to make the above Hamiltonian furthermore relevant for manganites, one needs to consider Hund's coupling between core t_{2g} spins and itinerant e_g electrons. This leads to invoking the double exchange mechanism for transport. Then, the hopping term $t_{i,j}$ between sites i and j in Eq. (1) is modified to be $t_{i,j}\sqrt{0.5[1+(\mathbf{S}_i\cdot\mathbf{S}_j/\mathbf{S}^2)]} = t_{i,j}\cos(\theta_{ij}/2)$ with $\mathbf{S}_i$ being the core t_{2g} spin at site i and θ_{ij} being the angle between $\mathbf{S}_i$ and $\mathbf{S}_j$. The term $\gamma^2_{\rm ep}t^2_{j,j+\delta}\cos^2(\theta_{ij}/2)/(g^2\omega_0)$ in Eq. (1) produces a strong ferromagnetic coupling between the spins at site j and site $j+\delta$ and this dominates over any superexchange coupling between the two spins.

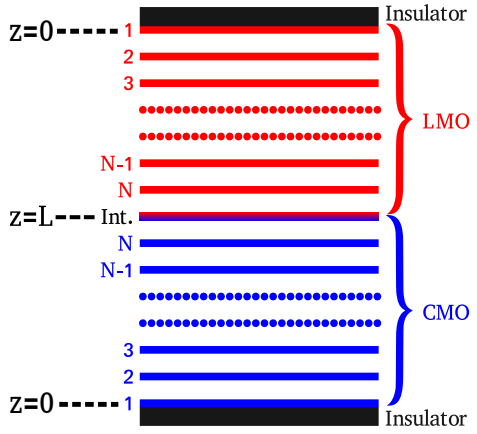

FIG. 1. (Color online) Schematic showing the symmetric (Insulator)/$(LaMnO_3)_N$/$(CaMnO_3)_N$/(Insulator) heterostructure. Each of the labeled N layers on both LMO ($LaMnO_3$) and CMO ($CaMnO_3$) sides, as well as in the Interface, comprise of manganese-oxide (MO) layers.

B. Charge Profile

To obtain the charge distribution, we ignore the effect of superexchange interaction in the starting effective Hamiltonian in Eq. (1) because its energy scale is significantly smaller than the polaronic energy term $2g^2\omega_0$. For a localized system, we only need to minimize the interaction energy which is a functional of the electronic density profile. The Coulombic interaction energy resulting from the electrons leaking from the LMO side to the CMO side, is taken into account by ascribing an effective charge +1 (hole) to the LMO unit cell (centered at the Mn site) that has donated an e_g electron from the Mn site and an effective charge −1 (electron) to the CMO unit cell (centered at the Mn site) that has accepted an e_g electron at the Mn site. The Coulombic energy that results is due to the interactions between these ±1 effective charges. The net positive charge on the LMO side and the net negative charge on the CMO side will produce a charge polarization (or inversion asymmetry). Since the ferroelectric dipole is expected to be in the direction perpendicular to the oxide-oxide (LMO-CMO) interface, we assume that the density is uniform in each layer for calculating the density profile as a function of distance z from the insulator-oxide interface. The Coulombic interaction energy per unit area due to leaked charges is the same for both LMO and CMO regions and is given, in the continuum approximation, to be

$$E_{\rm coul} = \frac{1}{8\pi\epsilon}\int_0^L dz D(z)^2, \tag{2}$$

where $D(z)$ is the electric displacement and is given by

$$D(z) = \pm\left[-\epsilon \mathrm{E}_{\rm ext} + \int_0^z dy 4\pi e\rho(y)\right], \tag{3}$$

with + (−) sign for LMO (CMO) side. Furthermore, $\rho(z)$ is the density of minority charges (i.e., holes on LMO side and electrons on SMO side), e the charge of a hole, ϵ the dielectric constant, $\mathrm{E}_{\rm ext}$ an external electric field along the z-direction, and L the thickness of the LMO (CMO) layers.

The ground state energy per unit area [corresponding to the effective Hamiltonian of Eq. (1)] can be written, in the continuum approximation, as a functional of $\rho(z)$ for both LMO and CMO as follows:

$$E_{\rm pol} = -\left[\gamma^1_{\rm ep}g^2\omega_0 + \frac{\gamma^2_{\rm ep}t^2}{g^2\omega_0}\right]\zeta\int_0^L dz\rho(z)[1-a^3\rho(z)], \tag{4}$$

where $\zeta = 6$ is the coordination number and a is the lattice constant. In arriving at the above equation we have approximated $n_{i+\delta}+n_{i-\delta}\approx 2n_i$. Furthermore, for the ground state, we expect $t_{ij}\sqrt{0.5[1+(\mathbf{S}_i\cdot\mathbf{S}_j/\mathbf{S}^2)]} = t_{ij}$, i.e., the minority charges will completely polarize the neighboring majority charges.

We will now minimize the total energy given below

$$E_{\rm Total} = 2E_{\rm pol} + 2E_{\rm coul}, \tag{5}$$

by setting the functional derivative $\delta E_{\rm Total}/\delta\rho(z) = 0$. This leads to the following equation

$$0 = -C_1[1-2a^3\rho(z)] + 2C_2\int_z^L dy\left[-\tilde{\mathrm{E}}_{\rm ext} + \int_0^y dx\rho(x)\right], \tag{6}$$

where $C_1 \equiv \left[\gamma^1_{\rm ep}g^2\omega_0 + \frac{\gamma^2_{\rm ep}t^2}{g^2\omega_0}\right]\zeta$; $C_2 \equiv 2\pi e^2/\epsilon$; and $\tilde{\mathrm{E}}_{\rm ext} \equiv \epsilon\mathrm{E}_{\rm ext}/(4\pi e)$. The above equation, upon taking double derivative with respect to z, yields

$$C_1 a^3\frac{d^2\rho(z)}{dz^2} - C_2\rho(z) = 0. \tag{7}$$

The above second-order differential Eq. (7) and Eq. (6) admit the solution

$$\rho(z) = \frac{1}{2a^3}\frac{\cosh(\xi z)}{\cosh(\xi L)} + \xi\tilde{\mathrm{E}}_{\rm ext}\frac{\sinh[\xi(L-z)]}{\cosh(\xi L)}, \tag{8}$$

where $\xi = \sqrt{C_2/(C_1 a^3)}$. It is important to note that, for the manganese-oxide (MO) layer at the LMO-CMO interface (i.e., at $z = L$), the density is 0.5 electrons/site and that it is independent of the applied external electric field and the system parameters. Now, since each Mn site in the interface layer belongs to a unit cell that is half LMO and half CMO, one expects the density per site to be 0.5. Additionally, as the distance from the LMO-CMO interface increases, we observe from Eq. (8) as well as from Figs. 2 and 3 that for smaller values of C_1, the density falls more rapidly while the density change due to electric field rises faster. Furthermore, for realistic values of the parameters, the charge density rapidly changes as we move away from the oxide-oxide interface (i.e., after only a few layers from the interface) and attains values close to the bulk value [as illustrated in Figs. 2(a) and 3(a)]. Lastly, as required for zero values of the external field $\mathrm{E_{ext}}$, we get $\rho(0) \to 0$ when $L \to \infty$. Thus, although we used the continuum approximation, our obtained density profile is qualitatively realistic as it has the desired values at the extremes $z = L$ and $z = 0$ with the density away from the LMO-CMO interface rapidly falling for not too large values of ϵ.

The density profiles for both LMO and CMO sides depend only on ϵ, C_1 and $\mathrm{E_{ext}}$. For our calculations displayed in Fig. 2, we used the following values for the parameters: $a = 4$ Å; $\epsilon = 20$; $\mathrm{E_{ext}} = 300$ kV/cm and 400 kV/cm; and $C_1 = 0.24$. For Fig. 3, we employed $\mathrm{E_{ext}} = 100$ kV/cm and $C_1 = 0.31$, with the values for a and ϵ being the same as in Fig. 2. The values of C_1 in Figs. 2 and 3 were chosen based on $\omega_0 = 0.07$ eV; $g = 2$; and $t = 0.1$ eV.

C. Magnetization distribution

We will now obtain the magnetization for a heterostructure by considering its lattice structure unlike the case for the density profile where a continuum approximation was made. Thus we can take into account the possibility of antiferromagnetic (AFM) order besides being able to consider ferromagnetic (FM) order.

First, based on Ref. 36, we note that the bulk $\mathrm{La_{1-x}Ca_xMnO_3}$ (below the magnetic transition temperatures) is A-AFM for $0 \leq x \lesssim 0.1$ and a ferromagnet for $0.1 \lesssim x \lesssim 0.5$. Hence, we model the LMO side of the heterostructure as an A-AFM when hole concentrations are small; whereas at higher concentrations of holes which is less than 0.5, the holes dictate the magnetic order by forming magnetic polarons that polarize the A-AFM. Next, we note that for $0.5 \lesssim x \lesssim 1.0$, the $\mathrm{La_{1-x}Ca_xMnO_3}$ bulk system is always an antiferromagnet. Thus, from a magnetism point-of-view, the magnetic moment on the CMO side of the heterostructure is expected to be zero except in the vicinity of the interface where (due to proximity effect) it will be a ferromagnet and can be modeled using a percolation picture. Given the above scenario, as can be expected, we find that the ferromagnetic region on the LMO side can be drastically enhanced (at the expense of the A-AFM region) by an electric field inducing holes on the LMO side. On the other hand, the electric field has only a small effect on the percolating ferromagnetic cluster that is adjacent to the oxide-oxide interface

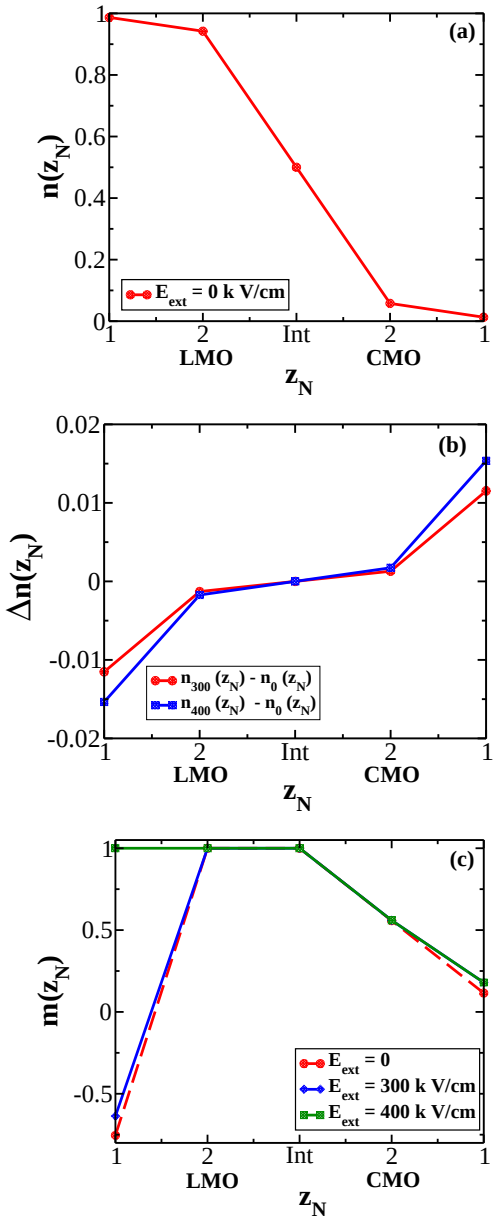

FIG. 2. (Color online) Electronic charge density $n(z_N)$ and per-site magnetization $m(z_N)$ (of t_{2g} spins normalized to unity) in various manganese-oxide layers of a (Insulator)/$(\mathrm{LaMnO_3})_2$/$(\mathrm{CaMnO_3})_2$/(Insulator) heterostructure for $a = 4$ Å, $\epsilon = 20$, and $C_1 = 0.24$. Figures are for (a) $n(\mathrm{E_{ext}} = 0$ kV/cm); (b) $\Delta n = n(\mathrm{E_{ext}} = 300/400$ kV/cm$) - n(\mathrm{E_{ext}} = 0$ kV/cm); and (c) $m(z_N)$ at $\mathrm{E_{ext}} = 0$ kV/cm, 300 kV/cm, and 400 kV/cm. MO layer 1 on the LMO side undergoes spin reversal when $\mathrm{E_{ext}} = 400$ kV/cm is applied.

on the CMO side.

1. CMO side

We will first consider the CMO side and show that the magnetization decays as we move away from the LMO-CMO interface. We derive below the largest FM domain; this domain percolates from the LMO-CMO interface. On account of nearest-neighbor repulsion (as given in Eq. (1)), the interface (which is half-filled) has e_g electrons on alternate sites. In fact, to minimize the interaction energy, on the CMO side we take the e_g electrons to be in one sublattice only which will be called e_g-sublattice; the other unoccupied sublattice will be called the u-sublattice. On account of virtual hopping, an e_g electron polarizes all its neighboring sites that do not contain any e_g electrons and forms a magnetic polaron. Thus we observe that the half-filled interface will be fully polarized and that there will be an FM cluster that begins at the interface and percolates to the layers away from the interface on the CMO side. For instance, in the layer next to the oxide-oxide interface, all the e_g electrons are in the same sublattice (the e_g-sublattice) and are next to the empty sublattice (i.e., sublattice unoccupied by e_g electrons) of the interface and hence are ferromagnetically aligned with the interface. Similarly, again in the layer adjacent to LMO-CMO interface, all the sites in the other sublattice (i.e., the u-sublattice) are empty and have the same polarization as the sites occupied by the e_g electrons at the interface.

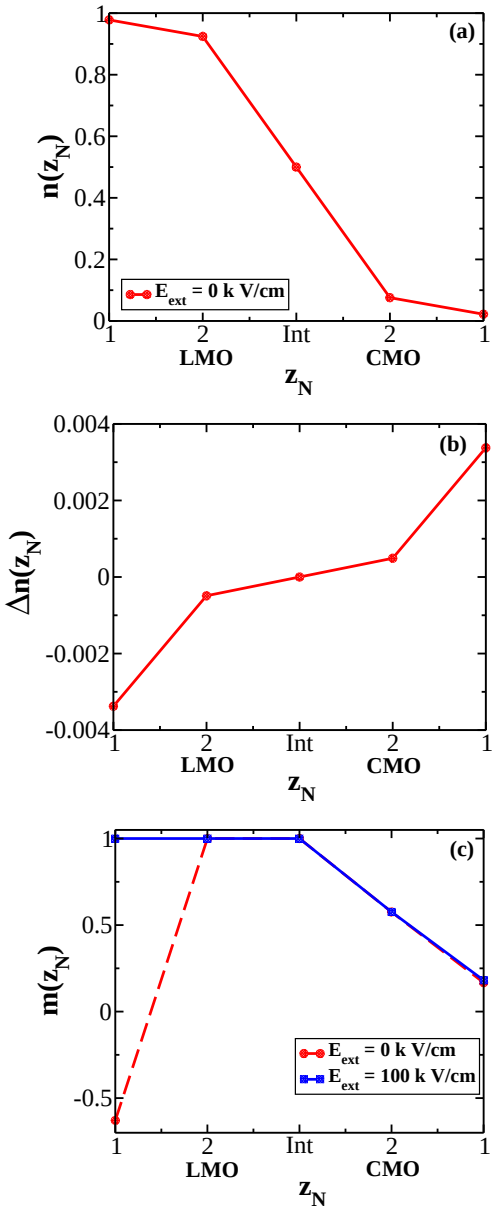

FIG. 3. (Color online) Electronic charge density $n(z_N)$ and per-site magnetization $m(z_N)$ (of normalized-to-unity t_{2g} spins) in various manganese-oxide layers of a (Insulator)/$(LaMnO_3)_2$/$(CaMnO_3)_2$/(Insulator) heterostructure for $a = 4$ Å, $\epsilon = 20$, and $C_1 = 0.31$. Plots pertain to (a) $n(\mathrm{E_{ext}} = 0$ kV/cm); (b) $\Delta n = n(\mathrm{E_{ext}} = 100$ kV/cm) − $n(\mathrm{E_{ext}} = 0$ kV/cm); and (c) $m(z_N)$ at $\mathrm{E_{ext}} = 0$ kV/cm and $\mathrm{E_{ext}} = 100$ kV/cm. The LMO side becomes completely ferromagnetic when $\mathrm{E_{ext}} = 100$ kV/cm is applied.

We will now identify the equations governing the ferromagnetic cluster percolating from the interface. Let z_N be the z-coordinate of the $\mathrm{N^{th}}$ 2D MO layer with N being the index measured from the Insulator-CMO interface (as shown in Fig. 1). Furthermore, we define $x_\mathrm{N}^{e_g}$ (x_N^{u}) as the concentration of polarized sites that belong to the spanning cluster and these sites are a subset of the sites in the e_g-sublattice (u-sublattice) in the $\mathrm{N^{th}}$ 2D MO layer. Then, the factor $(1-2x_\mathrm{N}^{e_g})$ $[(1-2x_\mathrm{N}^{u})]$ represents the probability of a site that belongs to the e_g-sublattice (u-sublattice) in layer N but is not part of the spanning polarized cluster. Now, the probability that a site, occupied (unoccupied) by an e_g electron, contributes to the FM cluster is equal to the probability of finding the site occupied (unoccupied) multiplied by 1-P where P is the probability that none of the adjacent sites that are in the u-sublattice (e_g-sublattice) belong to the percolating cluster. Therefore, we obtain the following set of coupled equations for the spanning cluster:

$$x_N^{e_g} = \rho(z_N)[1-(1-2x_{N-1}^{u})(1-2x_N^{u})^4(1-2x_{N+1}^{u})], \quad (9)$$

$$x_N^{u} = 0.5[1-(1-2x_{N-1}^{e_g})(1-2x_N^{e_g})^4(1-2x_{N+1}^{e_g})]. \quad (10)$$

The boundary conditions involving layer 1 are

$$x_1^{e_g} = \rho(z_1)[1-(1-2x_1^{u})^4(1-2x_2^{u})], \quad (11)$$

and

$$x_1^{u} = 0.5[1-(1-2x_1^{e_g})^4(1-2x_2^{e_g})], \quad (12)$$

while those for the LMO-CMO interface are $x_\mathrm{Int}^{e_g} = x_\mathrm{Int}^{u} = 0.5$.

2. LMO side

Next, we will show that the LMO side with only a few layers, for some realistic values of parameters, can have a sizeable change in the magnetism when a large electric field is applied and thus can be exploited to obtain a giant magneto-electric effect. Similar to the bulk situation in $LaMnO_3$[43,44], in our heterostructure as well, we assume that two spins on any adjacent sites in each MO layer have a ferromagnetic coupling $J_{xy} = 1.39$ meV; whereas, any two neighboring spins on adjacent layers have an antiferromagnetic coupling $J_z = 1.0$ meV. On the other hand, for an electron and a hole on neighboring sites either in the same MO layer or in adjacent MO layers, (due to virtual hopping of electron between the two sites) there is a strong ferromagnetic coupling $J_{eh} = \gamma_{ep}^2 t^2/(g^2\omega_0) >> J_{xy}$[42]. In our calculations, as long as the ratio of J_{xy}/J_z is taken as fixed and J_{eh} is the significantly dominant coupling, we get the same magnetic picture.

In a LMO side with a few MO layers, to demonstrate the possibility of large magnetization change upon the application of a large external field, we assume that the LMO-CMO interface and all MO layers up to layer M are completely polarized. Next, we assume that MO layers M and M-1 have low density of holes so that there is a possibility that spins in MO layer M-1 are not aligned with the block of MO layers starting from the LMO-CMO interface and up to layer M. We then analyze the polarization of MO layer M-1 by comparing the energies for the following two cases: (i) layers M-1 and M are antiferromagnetically aligned with the holes in layers M and M-1 inducing polarization only on sites that are adjacent to the holes; and (ii) MO layer M-1 is completely polarized and aligned with Layer M.

In a few-layered heterostructure (Insulator)/$(LaMnO_3)_2$/$(CaMnO_3)_2$/(Insulator), for $C_1 = 0.24$ eV [as shown in Fig. 2(c)] and for $C_1 = 0.31$ [as in Fig. 3(c)], we obtain a striking magneto-electric effect. For zero external field, when M = 2 is considered, case (i) (mentioned above) has lower energy, i.e., layer 1 is antiferromagnetically coupled to layer 2. On the other hand, when a strong electric field ($\sim$ 100 kV/cm for $C_1 = 0.24$ and $\sim$ 400 kV/cm for $C_1 = 0.31$) is applied, MO layer 1 (due to increased density of holes) becomes completely polarized and ferromagnetically aligned with the rest of the layers (i.e., MO layer 2 and the oxide-oxide interface) on the LMO side. Thus, we get a giant magneto-electric effect! We have considered C_1 values ranging from 0.24 to 0.31 and obtained magnetoelectric effect for various threshold electric field values. Changing C_1 is physically equivalent to changing the effective nearest-neighbor electron-hole attraction. Thus a smaller C_1 value of 0.24 indicates a lower effective nearest-neighbor electron-electron repulsion which requires a larger external electric field strength of 400 kV/cm to generate enough holes on the LMO side and, consequently, flip the magnetization of layer 1. Obviously, for the larger value $C_1 = 0.31$, sufficient number of holes are already present in the LMO system and layer 1 becomes ferromagnetic when a smaller E_{ext} (= 100 kV/cm) is applied. At still larger values of C_1, i.e., $C_1 \geq 0.32$, the LMO side is completely ferromagnetic even in the absence of an external field.

III. NUMERICAL APPROACH

Here, in this section, we construct a detailed 2D model Hamiltonian and study it numerically for the charge and magnetic profiles and the coupling between them.

A. Model Hamiltonian

In a quasi 2D heterostructure (involving only a few 2D layers of both manganites), as mentioned in Sec. II, we expect only a single narrow-width polaronic band to be relevant[42]. For our numerical treatment of a 2D lattice (with l_1 rows and l_2 columns), we employ the following one-band Hamiltonian:

$$H = H_{KE} + H_{pol}^{mf} + H_{SE} + H_{coul} + H_V. \quad (13)$$

The kinetic energy term H_{KE} is given by

$$H_{KE} = -te^{-g^2} \sum_{\langle i,j \rangle} \left[\cos\left(\frac{\theta_{ij}}{2}\right) c^\dagger{}_i c_j + \text{H.c.} \right], \quad (14)$$

where t is the hopping amplitude that is attenuated by the electron-phonon coupling g and c_j is the e_g electron destruction operator; furthermore, $\cos(\theta_{ij})$ is the modulation due to infinite Hund's coupling between the itinerant electrons and the localized t_{2g} spins with θ_{ij} being the angle between two localized $S = 3/2$ spins at sites i and j[45,46]. The second term H_{pol}^{mf} in Eq. (13) is the mean-field version of H_{pol} in Eq. (1) and is expressed as

$$H_{pol}^{mf} = \left[\gamma_{ep}^1 g^2 \omega_0 + \frac{\gamma_{ep}^2 t^2 \cos^2\left(\frac{\theta_{ij}}{2}\right)}{g^2\omega_0} \right] \times \sum_{i,\delta} \left[n_i - 2n_i \langle n_{i+\delta} \rangle + \langle n_i \rangle \langle n_{i+\delta} \rangle \right], \quad (15)$$

where $\langle n_i \rangle \equiv \langle c_i^\dagger c_i \rangle$ refers to the mean number density at site i. A derivation of $H_{KE} + H_{pol}$ is given in Ref. 41; however, for simplicity, here we have ignored the effect of next-nearest-neighbor hopping. The next term H_{SE} in Eq. (13) pertains to the superexchange[47] term which generates A-AFM in $LaMnO_3$ and G-AFM in $CaMnO_3$; thus on the $LaMnO_3$ side, it is given by

$$H_{SE}^{lmo} = -J_{xy} \sum_{\langle i,j \rangle_{xy}} \cos(\theta_{ij}) + J_z \sum_{\langle i,j \rangle_z} \cos(\theta_{ij}), \quad (16)$$

while on the $CaMnO_3$ side, we express it as

$$H_{SE}^{cmo} = J_z \sum_{\langle i,j \rangle} \cos(\theta_{ij}). \quad (17)$$

In the above superexchange expressions, the magnitude of the $S = 3/2$ spins is absorbed in the superexchange coefficients $J_{\rm xy}$ and $J_{\rm z}$. It should be clear that, away from the LMO-CMO interface, we can recover the spin arrangements of bulk $LaMnO_3$ and $CaMnO_3$; whereas, near the interface the minority carriers are expected to modify the spin textures. In Eq. (13), the Coulomb interaction is accounted for through the term $H_{\rm coul}$ as follows:

$$H_{\rm coul} = V_{\rm s}\sum_i n_i + \alpha t \sum_{i\neq j}\left[n_i\left(\frac{\langle n_j\rangle - Z_j}{|\vec{r}_i - \vec{r}_j|}\right) - \frac{\langle n_i\rangle\langle n_j\rangle}{2|\vec{r}_i - \vec{r}_j|}\right], \tag{18}$$

where the first term on the right hand side (RHS) is actually the on-site Coulomb interaction between an electron and a positive ion that yields the binding energy of an electron and is therefore applicable only to the LMO side. The remaining term on the RHS of Eq. (18), denotes long-range, mean-field Coulomb interactions between electrons as well as between electrons and positive ions. Here, Z_j represents the positive charge density operator with a value of either 1 or 0 and $|\vec{r}_i - \vec{r}_j|$ is the distance between lattice sites i and j. Furthermore, the dimensionless parameter $\alpha = \frac{e^2}{4\pi\epsilon a t}$ determines the strength of the Coulomb interaction. Lastly, in Eq. (13), the term $H_{\rm V}$ represents the potential felt at various sites due to an externally applied potential difference ($V_{\rm ext}$) between the two insulator edges (see Fig. 1):

$$H_{\rm V} = V_{\rm ext}\sum_{\rm I=1}^{l_2}\sum_{\rm K=1}^{l_1}\left[1 - \left(\frac{\rm I-1}{l_2-1}\right)\right] n_{\rm I+(K-1)}{}_{l_2}, \tag{19}$$

where I represents the layer (or column) index with l_2 denoting the number of layers, i.e., the number of sites in the z-direction; K represents the row index with l_1 denoting the number of rows, i.e., the number of sites in a layer.

B. Calculation procedure

We consider a 2D lattice involving a few layers (columns) of LMO and CMO and study magnetoelectric effect. The lattice does not have periodicity in the direction normal to the interface of the heterostructure (i.e., the z-direction). On the other hand, to mimic infinite extent in the direction parallel to the interface of the heterostructure, we assume periodic boundary condition in that direction. We employ classical Monte Carlo with Metropolis update algorithm to obtain the charge and magnetic profiles for our 2D lattice. To tackle the difficult problem of several local minima that are close in energy, we take recourse to the simulated annealing technique. To arrive at a reasonable charge profile at energy scales much larger than the superexchange energy scale, we treat the problem classically (i.e., fully electrostatically) by considering only the Coulomb term ($H_{\rm coul}$), the external-potential term ($H_{\rm V}$), and the electron-phonon-interaction term [$H^{\rm mf}_{\rm pol}(\theta_{ij} = 0)$] as these are the dominant energy terms in the Hamiltonian. The Coulomb term is subjected to mean-field analysis (as mentioned before) and the system generated potential $\alpha t \sum_{i\neq j}\left\{\frac{\langle n_j\rangle - Z_j}{|\vec{r}_i - \vec{r}_j|}\right\}$[48] in Eq. (18) is solved self-consistently. This is equivalent to solving the Poisson equation[49].

Next, to arrive at the final charge and magnetic configurations, we treat the system quantum mechanically by starting with an initial configuration comprising of the charge configuration generated classically (by the above procedure) and an initial random spin configuration. We now consider the full Hamiltonian, where hopping term ($H_{\rm KE}$) and spin interaction energy act as perturbation to the classical dominant energy terms [$H_{\rm coul}$, $H_{\rm V}$, and $H^{\rm mf}_{\rm pol}(\theta_{ij} = 0)$], thereby allowing for a small change in the number density profile and determine the concomitant magnetic profile. For the classical $t_{2\rm g}$ spins $\vec{S}_i = (\sin\theta_i\cos\phi_i, \sin\theta_i\sin\phi_i, \cos\theta_i)$ that are normalized to unity, the $\cos(\theta)$ and ϕ values are binned in the intervals $(-1, 1)$ and $(0, 2\pi)$ respectively with equally spaced 40 values of $\cos(\theta)$ and 80 values of ϕ, hence yielding a total of 3200 different possibilities.

In our calculations, we employ the parameter values $t = 0.1$ eV, $g = 2$ & 2.2, and $\omega_0 = 0.07$ leading to a small parameter value $\frac{t}{\sqrt{2}g\omega_0} < 1$. For our manganite heterostructure, lattice constant $a = 4$ Å, dielectric constant $\epsilon = 20$, magnetic couplings $J_{\rm z} = 1.00$ meV and $J_{\rm xy}/J_{\rm z} = 1.39$; we take the pre-factors [in Eq. (15)] $\gamma^1_{ep} = 0.3$ and $\gamma^2_{ep} = 0.25$. The coefficient in Eq. (18), representing the relative work function of the LMO side with respect to the CMO side, is taken to be $V_{\rm s} = 3\alpha$; hence the confining radius for the $e_{\rm g}$ electron is 1.33 Å which is less than half the lattice constant. External potential differences $V_{\rm ext}$, corresponding to external electric fields $\rm E_{ext} = 300$ kV/cm and $\rm E_{ext} = 400$ kV/cm (which are less than the breakdown field in LCMO[50]), are applied to study changes in the magnetization profiles.

The simulation (involving the charge and spin degrees of freedom) is carried out using exact diagonalization of the total Hamiltonian in Eq. (13). The spins are annealed over 61 values of the dimensionless temperature $[k_BT/(te^{-g^2})]$, in steps of 0.05, starting from 3 and ending at 0.05 with 15000 system sweeps carried out at each temperature. Since hopping energy $te^{-g^2} > J_{\rm xy}$, the inclusion of the spin degrees of freedom certainly commences at temperatures $k_BT > J_{\rm xy}$. Furthermore, the endpoint $k_BT = 0.05te^{-g^2}$ is sufficiently small to correspond to the ground state of the system. Each sweep requires visiting all the lattice sites sequentially and updating the spin configuration at each lattice site by the standard Metropolis Monte Carlo algorithm. We are also allowing the charge degrees of freedom to relax by treating the problem self-consistently. So, at the beginning of each sweep, the Poisson equation is solved additionally to make sure that the number densities have converged and

this is achieved with an accuracy of 0.001. Finally, averages of the various measurables in the system are taken over the last 5000 sweeps in the system.

C. Results and discussion

For numerical simulation, we consider two lattice sizes, namely, 12×6 and 12×8 with number of rows $l_1 = 12$ and number of layers (columns) $l_2 = 6$ or 8. Here, all the Mn sites in each layer belong solely to either LMO or CMO. This is in contrast to the continuum approximation employed in Sec. II B to obtain the charge profile analytically. In Sec. II B, by exploiting the symmetry of the interactions of the minority carriers on both sides of the LMO-CMO interface, we derived the charge profile with charge density always $\langle n \rangle = 0.5$ at the interface; this corresponds to a system comprising of odd number of MnO_2 layers with the interface MnO_2 layer being shared equally by the LMO and CMO sides, i.e., each Mn site (in the interface MnO_2 layer) belongs to a unit cell that is half LMO and half CMO.

We consider various situations in our lattices. First, we analyze the case of excluding electron-phonon interaction; consequently, the Hamiltonian of interest is that given by Eq. (13), but without the $H^{\rm mf}_{\rm pol}$ term. Next, we study the charge and magnetic profiles predicted by the total Hamiltonian of Eq. (13) for the symmetric situation (of equal number of LMO and CMO layers) and for different sizeable values of the electron-phonon coupling, i.e., for $g = 2$ & 2.2. Lastly, we examine the impact on the magnetoelectric effect due to the asymmetry in number of LMO and CMO layers.

1. *No electron-phonon interaction and* $\mathrm{E_{ext}} = 400$ kV/cm

Here, without the electron-phonon interaction, the hopping amplitude t is not attenuated by the factor e^{-g^2}

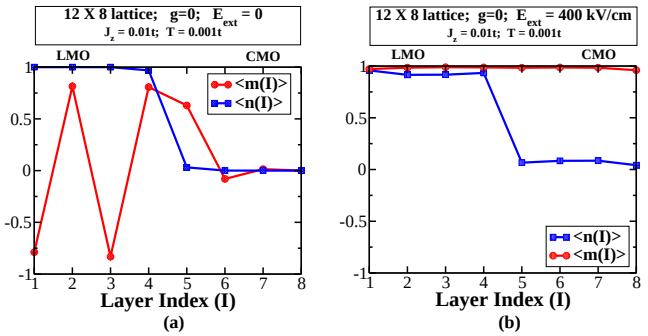

FIG. 4. (Color online) Layer-averaged charge density $\langle n(I) \rangle$ and layer-averaged per-site magnetization $\langle m(I) \rangle$ (of t_{2g} spins normalized to unity) for a symmetric 12×8 LMO-CMO lattice when electron-phonon interaction is zero; $J_z = 0.01t$ and $J_{xy}/J_z = 1.39$; $T = 0.001t$; and when (a) external electric field $E_{\rm ext} = 0$ and (b) $E_{\rm ext} = 400$ kV/cm.

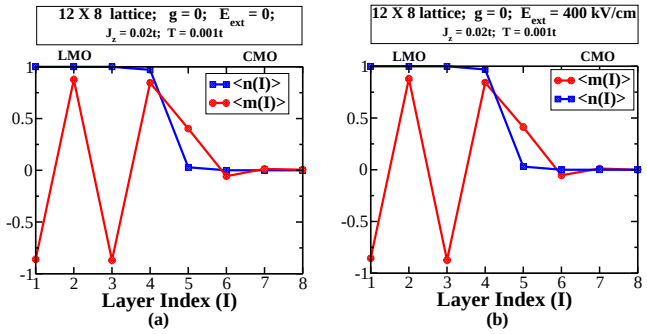

FIG. 5. (Color online) Layer-averaged charge density $\langle n(I) \rangle$ and layer-averaged per-site magnetization $\langle m(I) \rangle$ (of t_{2g} spins normalized to unity) for a symmetric 12×8 LMO-CMO lattice when electron-phonon interaction $g = 0$; superexchange $J_z = 0.02t$ and coupling ratio $J_{xy}/J_z = 1.39$; $T = 0.001t$; and when (a) $E_{\rm ext} = 0$ and (b) $E_{\rm ext} = 400$ kV/cm.

and the ground state is a superposition of various states in the occupation number representation. The electrons are not localized and we do not need to employ simulated annealing; the calculations were performed at a single temperature $k_B T = 0.001t$ on a symmetric heterostructure defined on a lattice with equal number of layers on the LMO side and the CMO side. Furthermore, the charge density profile is essentially dictated by the Coulombic term in Eq. (13); the kinetic term and the superexchange term have a negligible effect. Thus, we have density close to 1 on the LMO side and an almost zero density on the CMO side. Now, when a large electric field (400 kV/cm) is applied, a small amount of charge gets pushed across the interface. Then, since the kinetic term is much larger than the superexchange term, double exchange tries to ferromagnetically align the spins and, as shown in Fig. 4, we get a large change in the total magnetization of t_{2g} spins of the system, i.e., 0.91/site for the 12×8 lattice when t_{2g} spins are normalized to unity.

Keeping the temperature fixed at 0.001t, if we now double the value of J_z to 0.02t while retaining the magnetic-coupling ratio $J_{xy}/J_z = 1.39$, it is found that that the magnetoelectric effect disappears completely. Owing to the larger superexchage interaction, there is only a small change in the density on the LMO and CMO sides. Consequently, superexchange dominates over double exchange, thereby making the system totally antiferromagnetic (i.e., similar to the bulk, the LMO side is A-AFM and the CMO side is G-AFM). Furthermore, even after the application of a large external electric field (i.e., $E_{\rm ext} = 400$ kV/cm), there is practically no change in the magnetization as demonstrated in Fig. 5.

Next, on retaining the superexchange interaction values of $J_z = 0.01t$ and $J_{xy}/J_z = 1.39$, when the temperature is increased from 0.001t to 0.01t, the disordering effect of the temperature dominates over superexchange making the magnetic profile lose its oscillatory nature on the LMO side [as can be seen by comparing Fig. 6(a)

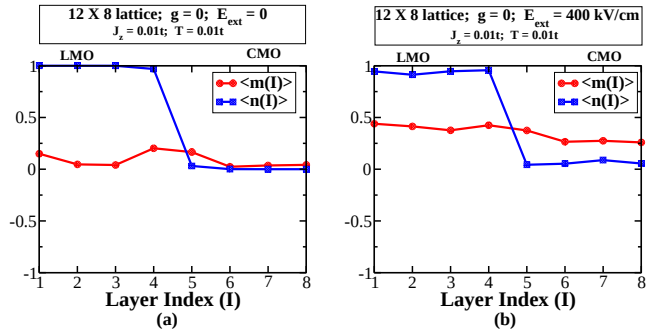

FIG. 6. (Color online) Layer-averaged charge density $\langle n(I)\rangle$ and layer-averaged per-site magnetization $\langle m(I)\rangle$ (of normalized-to-unity t_{2g} spins) for a symmetric 12×8 LMO-CMO lattice when $g = 0$; $J_z = 0.01t$ and $J_{xy}/J_z = 1.39$; enhanced temperature $T = 0.01t$; and when (a) $E_{ext} = 0$ and (b) $E_{ext} = 400$ kV/cm.

with Fig. 4(a)]. On the application of a sizeable external electric field (i.e., $E_{ext} = 400$ kV/cm), minority carrier density increases on both LMO and CMO sides. However, the disordering effect of the enhanced temperature diminishes the double exchange effect, thereby producing only a modest increase in the magnetization on both the LMO and CMO sides [see Fig. 6(b) and Fig. 4(b)].

In manganites the electron-phonon interaction is quite strong and leads to sizeable cooperative oxygen octahedra distortions. Hence, to get a more realistic picture, we switch on this interaction and study its effect on the system. Then, the hopping amplitude t is attenuated by the factor e^{-g^2} and the electrons are essentially localized. Consequently, the states are more or less classical in nature with number density at each site close to 1 (i.e., > 0.99 from our calculations) or close to 0 (i.e., < 0.01 from our numerics); the state of the system can be represented by a single state in the occupation number representation. As discussed in Sec. III B, we employ simulated annealing; we arrive at the charge and magnetic profiles reported in the subsequent Secs. III C 2–III C 6.

2. *Symmetric* 12×8 *lattice with* $g = 2.0$ *and* $E_{ext} = 300$ kV/cm

We now consider a symmetric 12×8 lattice with 4 layers of LMO and another 4 layers of CMO as shown in Fig. 7. We find charge modulation in the z-direction on both the sides, with neutral layers (free of minority carriers) sandwiched between charged layers (with minority carriers). The layers at the interface have the largest number of minority carriers with electrons and holes on alternate sites since contributions from both H_{pol} and H_{coul} [given by Eqs. (1) and (18)] are minimized for this arrangement. Layers 1 and 8, being the farthest from the LMO-CMO interface, are devoid of any minority carriers and retain the expected bulk charge distribution of LMO and CMO. We will now explain the charge modulation

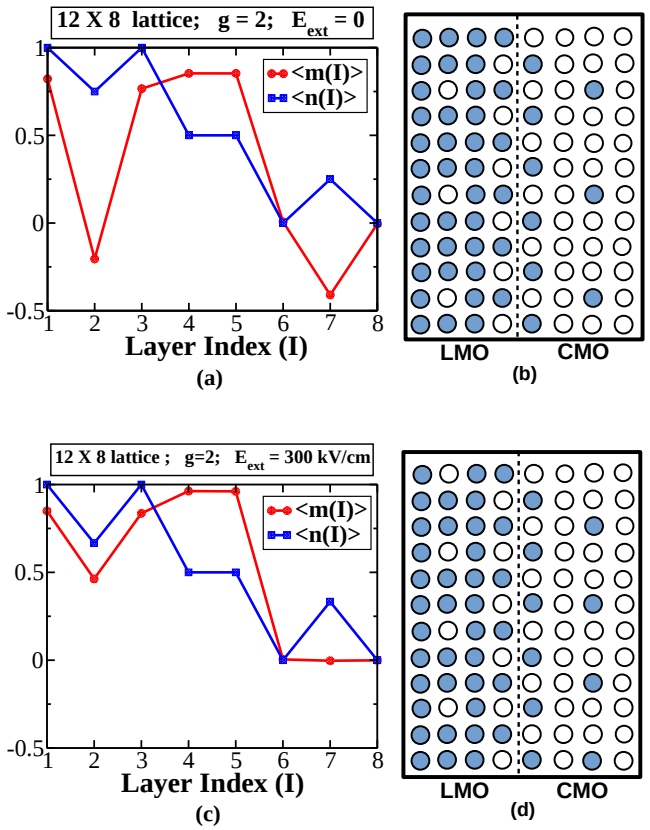

FIG. 7. (Color online) In a 12×8 symmetric lattice, when electron-phonon interaction strength $g = 2.0$, (a) when external electric field $E_{ext} = 0$, layer-averaged profiles of charge density $\langle n(I)\rangle$ and magnetization $\langle m(I)\rangle$ (of the t_{2g} spins normalized to unity); (b) when external electric field $E_{ext} = 0$, schematic occupation-number representation of ground state charge configuration in the lattice; (c) when a large external electric field $E_{ext} = 300$ kV/cm is applied, modified layer-averaged charge density $\langle n(I)\rangle$ and layer-averaged magnetization $\langle m(I)\rangle$ (of the t_{2g} spins normalized to unity) for various layers in the lattice; and (d) when $E_{ext} = 300$ kV/cm, reorganized ground state charge configuration.

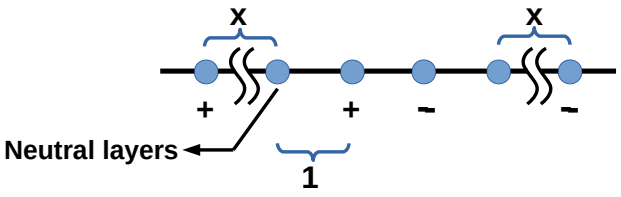

FIG. 8. (Color online) Charge modulation due to Coulomb interaction H_{coul} in a one-dimensional symmetric LMO-CMO lattice. The number of neutral layers/sites is x.

as follows. We compute the energy E_{coul} electrostatically for the one-dimensional chain in Fig. 8 using H_{coul} in Eq.(18), with lattice constant taken as unity and the

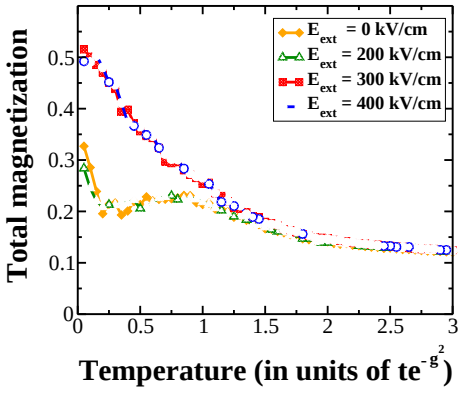

FIG. 9. (Color online) Total magnetization as a function of temperature for various $E_{\rm ext}$ in a 12×8 lattice when electron-phonon coupling $g = 2.0$. Figure shows that an enhancement in magnetization occurs for electric fields $E_{\rm ext} \gtrsim 300$ kV/cm; whereas below this threshold value, total magnetization does not change from its value at $E_{\rm ext} = 0$ kV/cm. The magnetoelectric effect is reasonably large at temperatures below $0.5te^{-g^2}$ (~ 10 K).

number of the neutral layers/sites as x. Then

$$E_{\rm coul} = \frac{1}{x+1} - \frac{1}{x+2} - \frac{1}{2x+3} - 1 - \frac{1}{x+2} + \frac{1}{x+1}$$
$$= \frac{2}{x+1} - \frac{2}{x+2} - \frac{1}{2x+3} - 1. \qquad (20)$$

If we plot $E_{\rm coul}$ as a function of x, we find that it drops rapidly till $x = 1$ and attains its minimum value gradually somewhere between $x = 6$ and $x = 7$. Similarly, we expect neutral layers to be present in 2D also and conclude that the charge ordering sets in due to electrostatic Coulomb energy minimization.

In Fig. 7, the interface is fairly polarized since the arrangement of electrons and holes on alternate sites produces a strong ferromagnetic coupling between the spins on these sites as $J_{\rm eh} >> J_{\rm xy} > J_{\rm z}$. Furthermore, again due to ferromagnetic couplings $J_{\rm eh}$ and $J_{\rm xy}$ on the LMO side, the interfacial layer polarizes the neutral layer 3 adjacent to it. Layer 1 is polarized in the direction of layer 3 due to antiferromagnetic coupling $J_{\rm z}$. On the CMO side, layer 6 is antiferromagnetic based on the charge configuration; layer 8, as expected, is also fully antiferromagnetic. As regards the case of zero electric field shown in Figs. 7(a) and 7(b), since layer 3 is antiferromagnetically connected to layer 2, layer 2 shows a small negative magnetization with the magnitude diminished due to the presence of a few (i.e., 3) holes in this layer. On the application of a large electric field $\rm E_{ext} = 300$ kV/cm, as displayed in Figs. 7(c) and 7(d), number of minority carriers increases in both layer 2 and layer 7. Consequently, the magnetization increases in these layers. On the application of the external electric field, there is an overall increase in the magnetization (of normalized-to-unity t_{2g} spins) by 0.17/site leading to a giant magnetoelectric effect (as can be seen in Fig. 9)

A study of the total magnetization with temperature for various external electric fields (i.e., $\rm E_{ext}$ increased in steps of 100 kV/cm from 0), as depicted in Fig. 9, reveals that we need a threshold field $\simeq 300$ kV/cm to get a fairly large increase in the total magnetization. Only above the threshold value, the density of minority charges increases and the resulting charge configuration is modified; correspondingly, the spin configuration gets altered too. Above 300 kV/cm, the charge configuration gets frozen for consecutive higher electric fields up to 600 kV/cm and no change in the magnetic profile can be expected. Although it may seem that much higher electric fields will further change the magnetization, they will actually produce a breakdown.

3. *Symmetric* 12×8 *lattice with* $g = 2.2$ *and* $\rm E_{ext} = 0$

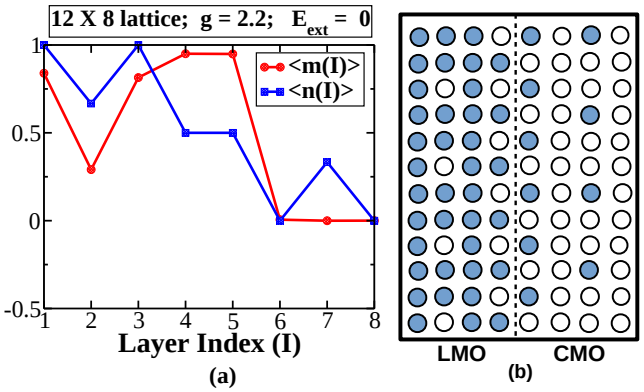

FIG. 10. (Color online) Result of enhanced electron-phonon coupling $g = 2.2$ and zero electric field, in a symmetric 12×8 lattice, on (a) layer-averaged charge density $\langle n(I)\rangle$ and layer-averaged magnetization $\langle m(I)\rangle$ (of the t_{2g} spins normalized to unity); and (b) ground state charge configuration.

Here we would like to point out that charge and magnetic profiles, when electron-phonon coupling g is strong and external electric field is zero, are similar to the profiles when coupling g is weak and external electric field is strong. In fact, as can be seen from Fig. 10 and Figs. 7(c) and 7(d), for $g = 2.2$ and $\rm E_{ext} = 0$ we get the same charge profile as when $g = 2.0$ and $\rm E_{ext} = 300$ kV/cm; the corresponding magnetic profiles in the two cases differ slightly because the ferromagnetic coupling values $J_{\rm eh} = \gamma_{\rm ep}^2 t^2/(g^2\omega_0)$ are slightly different.

4. *Symmetric* 12×6 *lattice with* $g = 2.2$ *and* $\rm E_{ext} = 400$ kV/cm

Since the electron-phonon interaction is stronger here (i.e., $g = 2.2$) compared to the situation in Sec. III C 2, even without the application of an external electric field, the concentration of minority carriers is higher (on both

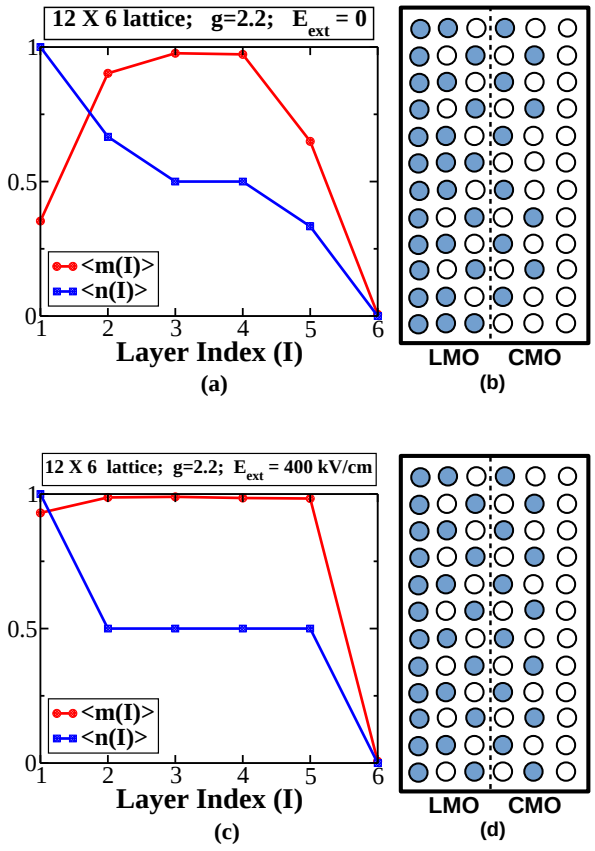

FIG. 11. (Color online) In a symmetric 12×6 lattice, for enhanced coupling $g = 2.2$, (a) at zero electric field, layer-averaged charge density $\langle n(I)\rangle$ and layer-averaged magnetization $\langle m(I)\rangle$ of t_{2g} spins normalized to unity; (b) at $\mathrm{E_{ext}} = 0$, ground state configuration; (c) at strong external electric field $\mathrm{E_{ext}} = 400$ kV/cm, layer-averaged charge density $\langle n(I)\rangle$ and layer-averaged magnetization $\langle m(I)\rangle$ of t_{2g} spins normalized to unity; and (d) at $\mathrm{E_{ext}} = 400$ kV/cm, charge configuration in the ground state.

LMO side and CMO side) as can be seen from Figs. 11 and 7. Again, as depicted in Figs. 11(a) and 11(b), the interfacial layers (i.e., layers 3 and 4) have electrons and holes on alternate sites resulting in full ferromagnetism. Here, we have fewer layers compared to the case in Sec. III C 2; there is no charge modulation in the z-direction because shifting the holes from layer 2 to layer 1 increases the number of nearest-neighbor repulsions due to electron-phonon interactions. Layers 2 and 5 also have a sizeable density of minority carriers (i.e., 1/3). Consequently, layer 2 is polarized due to its proximity to layer 3 and the ferromagnetic couplings J_{eh} and J_{xy}; contrastingly, the combination of J_{eh} and the antiferromagnetic coupling J_{z} lead to a smaller polarization in layer 5. Layer 1, due to its proximity to layer 2 (with sizeable concentration of holes) is also partially polarized. On the application of a large electric field ($\mathrm{E_{ext}} = 400$ kV/cm), as portrayed in Figs. 11(c) and 11(d), the concentration of holes further increases in layers 2 and 5 leading to fully ferromagnetically aligning these layers with layers 3 and 4. Furthermore, layer 1 also gets more polarized. On the whole, total magnetization (of normalized-to-unity t_{2g} spins) increases by ~ 0.17/site thus producing a giant magnetoelectric effect.

Lastly, it should be noted that (as expected) the magnetic profiles obtained here in Fig. 11 are quite similar to those in Figs. 2 and 3; on the other hand, the agreement between the charge profiles is not as good. On comparing the analytic treatment with the numerical approach, we note that the former makes a continuum approximation to obtain the charge profile. If the number of layers is large compared to the lattice constant, the continuum approximation is valid and the prediction of the analytic approach will agree with the more accurate numerical one. On the other hand, for a small system such as a 12×8 system, charge modulation is generated in the numerical approach unlike the analytic case.

5. *Asymmetric* 12×8 *system of 2 LMO layers and 6 CMO layers with* $g = 2.0$ *and* $\mathrm{E_{ext}} = 300$ kV/cm

We have an asymmetry here regarding the number of layers; the LMO side has two layers whereas the CMO side has six layers. For zero external electric field, as shown in Figs. 12(a) and 12(b), the two interfacial layers 2 and 3 contain perfectly alternate arrangement of electrons and holes; hence, the layers are fully polarized. Layer 1 is also ferromagnetically aligned with layer 2 because of their proximity. Beyond layer 3, similar to the G-AFM order in bulk CMO, the CMO side is antiferromagnetic, resulting in zero magnetization. Turning on the sizeable electric field $\mathrm{E_{ext}} = 300$ kV/cm, as depicted in Figs. 12(c) and 12(d), leads to a few electrons from layer 1 ending up in a farther layer 7; resultantly, the magnetic polarons in layer 7 partially polarize it. It is interesting to note that, here too charge modulation occurs due to the Coulomb term H_{coul} as demonstrated through Eq. (20). There is an overall increase in the magnetization (of normalized-to-unity t_{2g} spins) by 0.04/site; thus, the magnetoelectric effect is not huge.

6. *Asymmetric* 12×8 *system of 6 LMO layers and 2 CMO layers with* $g = 2.0$ *and* $\mathrm{E_{ext}} = 300$ kV/cm

Here, compared to the previous structure in Fig. 12, we have the opposite asymmetric structure of 6 LMO layers and 2 CMO layers (see Fig. 13). Due to the asymmetry connection between these two structures, we obtain a mirror image of the previous charge configuration for both with and without the external electric field. The interfacial layers 6 and 7, as expected, are totally ferromagnetic. Furthermore, layer 5 is also ferromagnetically aligned with layers 6 and 7 due to the ferromagnetic couplings J_{eh} and J_{xy}. At zero external field [as shown in Figs. 13(a) and 13(b)], similar to the bulk situation, we

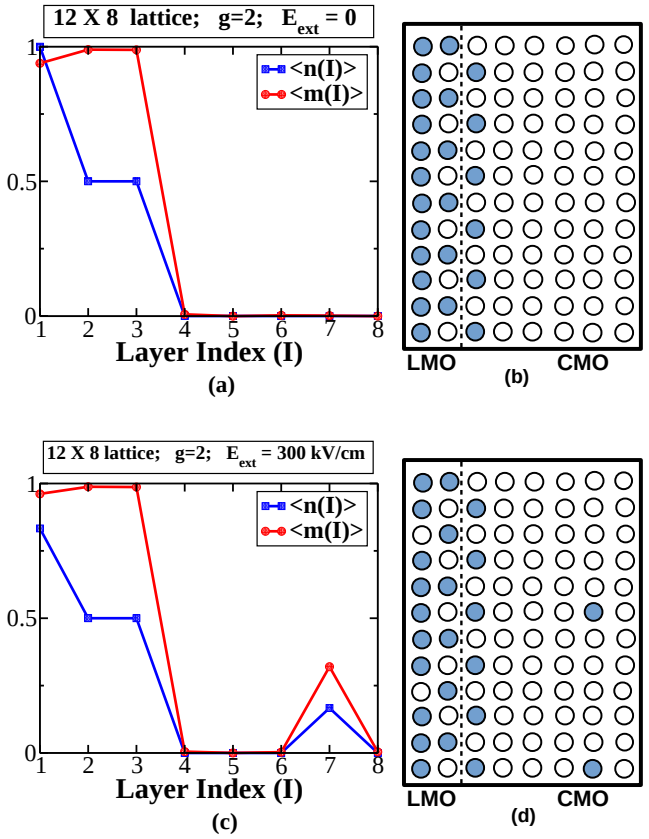

FIG. 12. (Color online) In asymmetric heterostructure defined on a 12 × 8 lattice with 2 layers of LMO and 6 layers of CMO, when coupling $g = 2.0$, (a) at $E_{ext} = 0$, layer-averaged charge density $\langle n(I)\rangle$ and layer-averaged magnetization $\langle m(I)\rangle$ of normalized-to-unity t_{2g} spins; (b) at $E_{ext} = 0$, ground state configuration; (c) at $E_{ext} = 300$ kV/cm, layer-averaged charge profile $\langle n(I)\rangle$ and layer-averaged magnetization profile $\langle m(I)\rangle$ of normalized-to-unity t_{2g} spins; and (d) at $E_{ext} = 300$ kV/cm, ground state configuration.

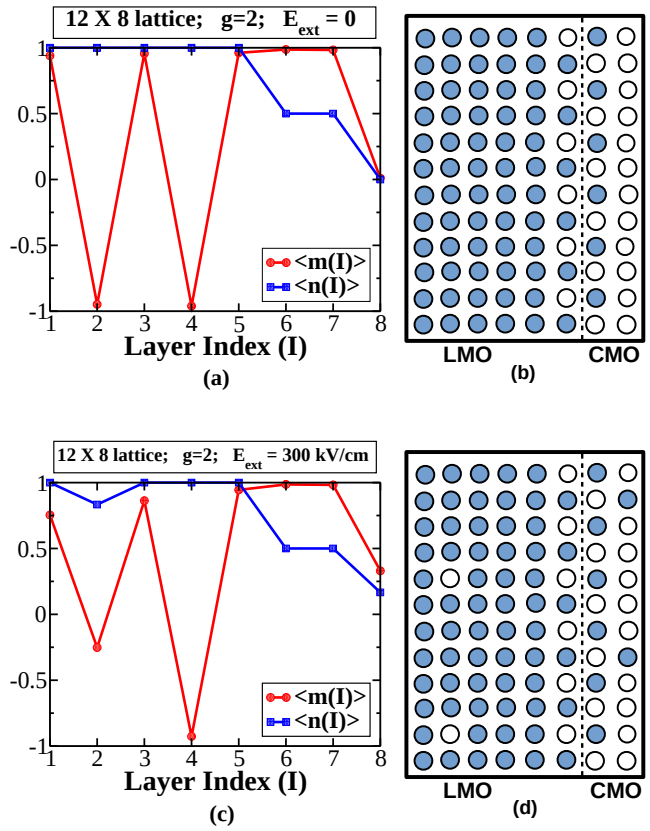

FIG. 13. (Color online) In asymmetric 12 × 8 lattice with 6 layers of LMO and 2 layers of CMO, when electron-phonon interaction $g = 2.0$, (a) at external electric field $E_{ext} = 0$, layer-averaged electron density $\langle n(I)\rangle$ and layer-averaged magnetization $\langle m(I)\rangle$ of t_{2g} spins normalized to unity; (b) at $E_{ext} = 0$, ground state electronic configuration; (c) at $E_{ext} = 300$ kV/cm, layer-averaged electron density $\langle n(I)\rangle$ and layer-averaged magnetization $\langle m(I)\rangle$ of t_{2g} spins normalized to unity; and (d) at $E_{ext} = 300$ kV/cm, ground state.

have A-AFM on the LMO side up to layer 5; layer 8, similar to the bulk CMO, is also antiferromagnetic. The minority carriers, generated due to the external electric field $E_{ext} = 300$ kV/cm [as shown in Figs. 13(c) and 13(d)], produce magnetic polarons which increase the polarization. There is an overall increase in the magnetization (of normalized-to-unity t_{2g} spins) by about 0.1/site implying a large magnetoelectric effect.

From the various symmetric and asymmetric LMO-CMO configurations considered, we conclude that the symmetric arrangement yields the largest magnetoelectric effect.

IV. CONCLUSIONS

We used the heuristic notion that, when the two Mott insulators LMO and CMO are brought together to form a heterostructure, one may realize the entire phase diagram of $La_{1-x}Ca_xMnO_3$ across the heterostructure with the $x = 0$ phase occurring at the LMO surface at one end and evolving to the $x = 0.5$ state at the oxide-oxide interface and finally to the $x = 1$ phase at the other end of CMO. However, owing to the reduced dimensions (namely, quasi two-dimensions), we expect only A-AFM and FMI phases on the LMO side. On enhancing the minority carrier density (on both sides of the interface) by using a sizeable external electric field, we showed that the FMI region can be further expanded at the expense of the A-type AFM region on the LMO side and the G-AFM domain on the CMO side, thereby producing a giant magnetoelectric effect. It is important to note that the system behaves like an anisotropic Coulombic solid: for a given average density in a layer, the minority charges by and large order periodically and as far apart as possible; the Coulombic interaction dictates how the charge arrangement of one layer adjusts itself with respect to the configuration in another layer. Furthermore, the two layers at the interface are ferromagnetically ordered as

they are at half-filling. When electric fields are introduced in the system, the minority charge density away from the interface gets enhanced leading to charge reordering; consequently, the magnetization away from the interface changes layer by layer resulting in an increase in the total ferromagnetic moment. This scenario is key to the understanding of the magnetoelectric effect.

As a guide to designing magnetoelectric devices, we find that symmetric heterostructures with equal number of LMO and CMO layers yield larger magnetoelectric effect compared to asymmetric heterostructures with unequal number of LMO and CMO layers. It should also be noted that this heterostructure/device can be used near helium liquefaction temperatures; on the other hand, the magnetoelectric function disappears before nitrogen liquefaction temperature is attained.

We also would like to mention that if a superlattice were formed from the heterostructure (Insulator)/$(LaMnO_3)_n$/$(CaMnO_3)_n$/(Insulator), then the dipoles from each repeating heterostructure unit will add up to produce a giant electric dipole moment; furthermore, this superlattice will also realize a giant magnetoelectric effect. On the other hand, if the insulator layers were not present, the superlattice formed from the repeating unit $(LaMnO_3)_n$/$(CaMnO_3)_m$ would not produce a large electric dipole as the charge from LMO can leak to CMO on both sides leading to a small net dipole moment. More importantly, the $(LaMnO_3)_n$/$(CaMnO_3)_m$ superlattice will also not generate a giant magnetoelectric effect as an applied electric field will not alter much the total amount of charge in LMO or CMO; this is because charge leaked by LMO to CMO on one side is replaced by CMO on the other side.

Based on the above arguments, it should be clear that, compared to experiments involving superlattices where alloy/bulk effect vanishes when the thinner side of the repeating unit has more than two layers, in our heterostructure bulk nature should vanish when the thinner side has more than 1 layer. Thus, in the superlattice $(LaMnO_3)_{2n}$/$(SrMnO_3)_n$ studied in Ref. 21, the metallic behavior (corresponding to bulk $La_{0.67}Sr_{0.33}MnO_3$) disappears for $n > 2$ and is replaced by insulating behavior; whereas, in the heterostructure (Insulator)/$(LaMnO_3)_{2n}$/$(SrMnO_3)_n$/(Insulator) we expect insulating behavior for $n > 1$. This observation supports our assumption that, in our quasi 2D LMO-CMO heterostructures (corresponding to LCMO that has a narrower band width and a stronger electron-phonon coupling compared to LSMO), only a single narrow-width polaronic band is pertinent. Additionally, interfacial roughness (if considered) will further reduce the band width and suppress metallicity.

Lastly, it should also be pointed out that, in a realistic situation, we have electron-electron repulsion (produced by cooperative electron-phonon interaction) and double-exchange generated ferromagnetic coupling extending to next-nearest-neighbor sites[51] leading to a larger magnetic polaron and thus producing a stronger magnetoelectric effect compared to what our calculations reveal.

V. ACKNOWLEDGEMENTS

S. Y. acknowledges discussions with T. V. Ramakrishnan, D. D. Sarma, and K. Pradhan. S. P. acknowledges discussions with S. Nag, R. Ghosh, S. Kadge, N. Swain, S. Mukherjee, and R. Raman. Work at Argonne National Laboratory is supported by the U.S. Department of Energy, Basic Energy Sciences Materials Science and Engineering, under contract no. DE-AC02-06CH11357.

[1] C. H. Ahn, A. Bhattacharya, M. Di Ventra, J. N. Eckstein, C. Daniel Frisbie, M. E. Gershenson, A. M. Goldman, I. H. Inoue, J. Mannhart, Andrew J. Millis, Alberto F. Morpurgo, Douglas Natelson, and Jean-Marc Triscone, Rev. Mod. Phys. **78**, 1185 (2006).

[2] J. Chakhalian, J. W. Freeland, A. J. Millis, C. Panagopoulos, and J. M. Rondinelli, Rev. Mod. Phys. **86**, 1189 (2014).

[3] One striking example is the interface of $LaAlO_3/SrTiO_3$ system reported in A. Ohtomo and H. Y. Hwang, Nature **427**, 423 (2004); N. Reyren, S. Thiel, A. D. Caviglia, L. Fitting-Kourkoutis, G. Hammerl, C. Richter, C. W. Schneider, T. Kopp, A.-S. Rüetschi, D. Jaccard, M. Gabay, D. A. Muller, J.-M. Triscone, and J. Mannhart, Science **317**, 1196 (2007); A. Brinkman, M. Huijben, M. van Zalk, J. Huijben, U. Zeitler, J. C. Maan, W. G. van der Wiel, G. Rijnders, D. H. A. Blank, and H. Hilgenkamp, Nat. Mater. **6**, 493 (2007); D. A. Dikin, M. Mehta, C. W. Bark, C. M. Folkman, C. B. Eom, and V. Chandrasekhar, Phys. Rev. Lett. **107**, 056802 (2011); N. C. Bristowe, Emilio Artacho, P. B. Littlewood, Phys. Rev. B **80**, 045425 (2009); N. C. Bristowe, P. B. Littlewood, Emilio Artacho, J. Phys.: Condens. Matter **23**, 081001 (2011).

[4] J. Mannhart and D. G. Schlom, Science **327**, 1607 (2010).

[5] H. Boschker and J. Mannhart, arXiv:1607.07239v1.

[6] H. Takagi and H. Y. Hwang, Science **327**, 1601 (2010).

[7] G. Hammerl and N. Spaldin, Science **332**, 922 (2011).

[8] H. Y. Hwang, Y. Iwasa, M. Kawasaki, B. Keimer, N. Nagaosa, and Y. Tokura, Nat. Mater. **11**, 103 (2012).

[9] E. Dagotto, Science **318**, 1076 (2007).

[10] L. W. Martin and R. Ramesh, Acta Materialia **60**, 2449 (2012)

[11] For a review see J. P. Velev, S. S. Jaswal and E. Y. Tsymbal, Phil. Trans. R. Soc. A **369**, 3069 (2011).

[12] D. I. Khomskii, J. Magn. Magn. Mater, **306**, 1 (2006).

[13] D. Khomskii, Phys. **2**, 20 (2009).

[14] K. F. Wang, J. M. Liu, and Z. F. Ren, Adv. Phys. **58**, 321 (2009).

[15] M. Fiebig and N. A. Spaldin, Eur. Phys. J. B **71**, 293 (2009).

[16] P. Yu, Y.-H. Chu, and R. Ramesh, Mater. Today **15**, 320 (2012).
[17] X. Huang and S. Dong, Mod. Phys. Lett. B **28**, 1430010 (2014).
[18] J. M. Rondinelli, M. Stengel, and N. A. Spaldin, Nat. Nanotechnol. **3**, 46 (2008).
[19] M. K. Niranjan, J. D. Burton, J. P. Velev, S. S. Jaswal, and E. Y. Tsymbal, Appl. Phys. Lett. **95**, 052501 (2009).
[20] J. D. Burton and E. Y. Tsymbal, Phys. Rev. B **80**, 174406 (2009).
[21] A. Bhattacharya, S. J. May, S. G. E. te Velthuis, M. Warusawithana, X. Zhai, Bin Jiang, J.-M. Zuo, M. R. Fitzsimmons, S. D. Bader, and J. N. Eckstein, Phys. Rev. Lett. **100**, 257203 (2008).
[22] Ş. Smadici, P. Abbamonte, A. Bhattacharya, X. Zhai, B. Jiang, A. Rusydi, J. N. Eckstein, S. D. Bader, and J.-M. Zuo, Phys. Rev. Lett. **99**, 196404 (2007).
[23] S. J. May, A. B. Shah, S. G. E. te Velthuis, M. R. Fitzsimmons, J. M. Zuo, X. Zhai, J. N. Eckstein, S. D. Bader, and A. Bhattacharya, Phys. Rev. B **77**, 174409 (2008).
[24] A. Bhattacharya, X. Zhai, M. Warusawithana, J. N. Eckstein, and S. D. Bader, Appl. Phys. Lett. **90**, 222503 (2007).
[25] C. Adamo, X. Ke, P. Schiffer, A. Soukiassian, M. Warusawithana, L. Maritato, and D. G. Schlom Appl. Phys. Lett. **92**, 112508 (2008).
[26] T. Koida, M. Lippmaa, T. Fukumura, K. Itaka, Y. Matsumoto, M. Kawasaki, and H. Koinuma, Phys. Rev. B **66**, 144418 (2002).
[27] H. Yamada, M. Kawasaki, T. Lottermoser, T. Arima, and Y. Tokura, Appl. Phys. Lett. **89**, 052506 (2006).
[28] E. J. Monkman, C. Adamo, J. A. Mundy, D. E. Shai, J. W. Harter, D. Shen, B. Burganov, D. A. Muller, D. G. Schlom, and K. M. Shen, Nat. Mater. **11**, 855 (2012).
[29] C. Lin, S. Okamoto, and A. J. Millis, Phys. Rev. B **73**, 041104(R) (2006).
[30] C. Lin and A. J. Millis, Phys. Rev. B **78**, 184405 (2008).
[31] B. R. K. Nanda and S. Satpathy, Phys. Rev. B **78**, 054427 (2008).
[32] S. Dong, R. Yu, S. Yunoki, G. Alvarez, J.-M. Liu, and E. Dagotto, Phys. Rev. B **78**, 201102(R) (2008).
[33] R. Yu, S. Yunoki, S. Dong, E. Dagotto , Phys. Rev. B **80** 125115 (2009).
[34] C. Adamo, C. A. Perroni, V. Cataudella, G. De Filippis, P. Orgiani, and L. Maritato, Phys. Rev. B **79**, 045125 (2009).
[35] Y. Tokura, Rep. Prog. Phys. **69**, 797 (2006).
[36] See K.H. Kim, M. Uehara, V. Kiryukhin and S.-W. Cheong, in *Colossal Magnetoresistive Manganites*, edited by T. Chatterji, (Kluwer Academic, Dordrecht, 2004).
[37] C. Martin, A. Maignan, M. Hervieu, and B. Raveau, Phys. Rev. B **60**, 12191 (1999).
[38] K. Pradhan and A. P. Kampf, Phys. Rev. B **88**, 115136 (2013); J. Salafranca, M. J. Calderón, and L. Brey, Phys. Rev. B **77**, 014441 (2008); D. Niebieskikwiat, L. E. Hueso, J. A. Borchers, N. D. Mathur, and M. B. Salamon Phys. Rev. Lett. **99**, 247207 (2007).
[39] S. Datta, A. Das, and S. Yarlagadda, Phys. Rev. B **71**, 235118 (2005).
[40] S. Reja, S. Yarlagadda, and P. B. Littlewood, Phys. Rev. B **84**, 085127 (2011).
[41] R. Pankaj and S. Yarlagadda, Phys. Rev. B **86**, 035453 (2012).
[42] G. V. Pai, S. R. Hassan, H. R. Krishnamurthy, and T. V. Ramakrishnan, Europhys. Lett. **64**, 696 (2003); T. V. Ramakrishnan, H. R. Krishnamurthy, S. R. Hassan, and G. V. Pai, Phys. Rev. Lett. **92**, 157203 (2004).
[43] N. N. Kovaleva, Andrzej M. Oleś, A. M. Balbashov, A. Maljuk, D. N. Argyriou, G. Khaliullin, and B. Keimer, Phys. Rev. B **81**, 235130 (2010).
[44] K. Hirota, N. Kaneko, A. Nishizawa, and Y. Endoh, J. Phys. Soc. Jpn. **65**, 3736 (1996); F. Moussa, M. Hennion, J. Rodríguez-Carvajal, H. Moudden, L. Pinsard, and A. Revcolevschi, Phys. Rev. B **54**, 15149 (1996); G. Biotteau, M. Hennion, F. Moussa, J. Rodríguez-Carvajal, L. Pinsard, A. Revcolevschi, Y. M. Mukovskii, and D. Shulyatev, *ibid.* **64**, 104421 (2001).
[45] P. -G. de Gennes, Phys. Rev. **118**, 141 (1960).
[46] Y. A. Izyumov, Y. N. Skryabin, Phys.-Usp. **44**, 109 (2001).
[47] P. W. Anderson, Phys. Rev. **115**, 2 (1959).
[48] S. Okamoto and A. J. Millis, Phys. Rev. B **70**, 075101 (2004).
[49] S. Yunoki, A. Moreo, E. Dagotto, S. Okamoto, S. S. Kancharla, and A. Fujimori, Phys. Rev. B 76, 064532 (2007).
[50] T. Wu, S. B. Ogale, J. E. Garrison, B. Nagaraj, A. Biswas, Z. Chen, R. L. Greene, R. Ramesh, T. Venkatesan, and A. J. Millis, Phys. Rev. Lett. **86**, 5998 (2001).
[51] R. Pankaj and S. Yarlagadda, arXiv:1608.06055.